Space-Time Multiscale Model for Wave Propagation in Heterogeneous Media

Jacob Fish and Wen Chen

Rensselaer Polytechnic Institute

Abstract: A space-time multiscale model for wave propagation in heterogeneous media is developed. The model builds on the authors' previous work on the higher-order mathematical homogenization theory with multiple spatial and temporal scales, and is aimed at addressing the issues of stability and mathematical consistency. Starting from the weak forms of homogenized macroscopic equations of motion, terms causing the solution secularity are identified and enforced to vanish. This condition recovers the missing boundary conditions and gives rise to two secularity constrains imposing the uniform validity of asymptotic expansions. Finite element semidiscretization in space along with an analytical solution in time are employed to incorporate the secularity constrains in the leading-order solution and account for the slow time dependence of the leading solution. Pade approximation is utilized to develop the time stepping schemes on the fast time scale. The formulation is verified for wave propagation problems in semi-infinite and finite domains.

Key words: wave propagation, heterogeneous medium, space-time homogenization, multiple scales, Pade approximation.

1.0 Introduction

This manuscript is partially motivated by the fact that recent experiments conducted on composite tubes [1] showed a clear tendency toward lower strain energy absorption at higher crush rates - a surprising phenomenon that cannot be explained by current modeling and simulation practices. Impact of structural systems with sizeable microstructure is a complex multiscale phenomenon in both space and time and yet existing modeling and simulation tools are phenomenological in nature. In our previous studies we have shown ([2]-[5]) that existence of multiple temporal scales is one of the main causes for lower strain energy absorption at high strain rates. Classical homogenization-based, nonlocal and phenomenological models, such as Model 58 in LS-Dyna3D [20], err badly in comparison to both the reference solution obtained by modeling the problem on the scale of heterogeneity and the experimental data [1]. In ([2]-[5]) we have shown that multiple temporal scales give rise to the augmentation of the mass matrix. The added mass term has been shown ([2]-[5]) to be positive definite and the multiscale formulation in space and time translates into lower strain energy absorption at high strain rates.

The nonlocal formulation developed in ([2]-[5]) is not without shortcomings: (i) it is unstable for high frequency excitations, (ii) it gives rise to fourth order differential equation with insufficient boundary conditions and, (iii) it results in poor predictions of wave reflections from boundaries. In [6][10] a nonlocal three-field Hamilton variational principle has been developed to construct a high frequency filter aimed at stabilizing the nonlocal equations of motion. Nevertheless, the computational complexity of the nonlocal mixed formulation is substantial; the issue of missing boundary conditions has not been fully resolved; and the problem of wave reflection from the boundaries has not been adequately addressed.

The present manuscript is an extension of the authors' previous work ([4]-[6]) and is aimed at circumventing the deficiencies observed in the previous formulation. Starting from the weak forms of homogenized macroscopic equations of motion ([4]-[6]), we identify the terms which give rise to the solution secularity and enforce them to vanish. This condition recovers the missing boundary conditions and gives rise to two secularity constrains imposing the uniform validity of asymptotic expansions. The secularity constrains are closely related to higher order equilibrium equations of Fleck and Hutchinson [7]. Finite element semidiscretization in space along with an analytical solution in slow time scales and Pade approximation in fast time scale are employed. The formulation is verified for wave propagation problems in semi-infinite and finite domains.

2.0 Synopsis of the Previous Work

2.1 Higher-order homogenization with multiple space-time scales

We consider the problem of elastodynamics of a heterogeneous solid with periodic microstructure governed by the following equations

$$\rho\ddot{u}_i - \sigma_{ij,j} = 0, \quad \sigma_{ij} = C_{ijkl}e_{kl}, \quad e_{ij} = \frac{1}{2}(u_{i,j} + u_{j,i}), \text{ in } \Omega, \tag{1}$$

with initial-boundary conditions:

$$u_i(\boldsymbol{x}, t = 0) = p_i(\boldsymbol{x}), \quad \dot{u}_i(\boldsymbol{x}, t = 0) = g_i(\boldsymbol{x}), \text{ in } \Omega, \tag{2}$$

$$u_i = \bar{u}_i \text{ on } \Gamma_u; \quad \sigma_{ij}n_j = \bar{h}_i \text{ on } \Gamma_\sigma. \tag{3}$$

where Ω denotes the macroscopic domain of interest with boundary $\Gamma = \Gamma_u \bigcup \Gamma_\sigma$, $\Gamma_u \bigcap \Gamma_\sigma = \varnothing$; u_i is the displacement field, e_{ij} the small strain tensor, σ_{ij} the stress tensor, C_{ijkl} the elasticity tensor and ρ the mass density. The elasticity tensor and mass density are assumed to be locally periodic with a period denoted as Y. We assume that micro-constituents possess homogeneous properties and satisfy equilibrium, constitutive, kinematics and compatibility equations as well as jump conditions at the interface between the micro-phases.

On the premise that the dimension of the heterogeneity l is significantly smaller than the characteristic size of the macroscopic problem $L = \lambda/(2\pi)$, with λ denoting the wavelength of the traveling signal, i.e., $0 < l/L = \varepsilon \ll 1$, we introduce the macro- and micro-coordinate systems $\boldsymbol{x}$ and $\boldsymbol{y}$, such that

$$\boldsymbol{y} = \boldsymbol{x}/\varepsilon. \tag{4}$$

In addition to the multiple spatial scales, the following multiple temporal scales are introduced [4][5]

$$t_0 = t, \quad t_1 = \varepsilon t, \quad t_2 = \varepsilon^2 t, \tag{5}$$

where t_0 is the usual time scale, t_1 and t_2 are the slow time scales.

Using the chain rule, the spatial and temporal derivatives can be expressed as

$$(\ )_{,i} = (\ )_{,x_i} + \varepsilon^{-1}(\ )_{,y_i}, \quad \dot{(\ )} = (\ )_{,t_0} + \varepsilon(\ )_{,t_1} + \varepsilon^2(\ )_{,t_2}, \tag{6}$$

where the superposed dot denotes the full time derivative.

The displacement field is approximated using multiple-scale asymptotic expansion in the form

$$u_i(\boldsymbol{x}, \boldsymbol{y}, t) = u_i^0(\boldsymbol{x}, \boldsymbol{y}, t_0, t_1, t_2) + \varepsilon u_i^1(\boldsymbol{x}, \boldsymbol{y}, t_0, t_1, t_2) + \varepsilon^2 u_i^2(\boldsymbol{x}, \boldsymbol{y}, t_0, t_1, t_2) + \ldots \tag{7}$$

Substituting equation (7) into the governing equation (1) and identifying terms with equal power of ε yields equilibrium equations at different orders. As a consequence of linearity and periodicity, the general solutions to $\boldsymbol{u}^0$, $\boldsymbol{u}^1$ and $\boldsymbol{u}^2$ take the following form

$$u_i^0(\boldsymbol{x}, \boldsymbol{y}, t_0, t_1, t_2) = u_i^0(\boldsymbol{x}, t_0, t_1, t_2),$$

$$u_i^1(\boldsymbol{x}, \boldsymbol{y}, t_0, t_1, t_2) = U_i^1(\boldsymbol{x}, t_0, t_1, t_2) + H_{ikl}(\boldsymbol{y}) e_{xkl}(\boldsymbol{u}^0),$$

$$u_i^2(\boldsymbol{x}, \boldsymbol{y}, t_0, t_1, t_2) = U_i^2(\boldsymbol{x}, t_0, t_1, t_2) + H_{ikl}(\boldsymbol{y}) e_{xkl}(\boldsymbol{U}^1) + P_{ijmn}(\boldsymbol{y})(e_{xmn}(\boldsymbol{u}^0))_{,x_j}, \tag{8}$$

where $e_{xkl}(\boldsymbol{u}) = (u_{k,x_l} + u_{l,x_k})/2$ is the macroscopic symmetric gradient of $\boldsymbol{u}$; $\boldsymbol{H}$ and $\boldsymbol{P}$ are Y-periodic third- and fourth-rank tensors, respectively, which can be determined by solving the following unit cell boundary value problems (see for example [2]-[6]):

$$C_{ijmn,y_j}^0 = 0, \quad C_{ijmn}^0(\boldsymbol{y}) = C_{ijkl}(G_{klmn} + \delta_{mk}\delta_{nl}), \tag{9}$$

$$C_{ijpmn,y_j}^1 = \theta(\boldsymbol{y}) D_{ipmn}^0 - C_{ipmn}^0(\boldsymbol{y}), \quad C_{ijpmn}^1(\boldsymbol{y}) = C_{ijpk} H_{kmn} + C_{ijkl} B_{klpmn}, \tag{10}$$

where

$$G_{klmn}(\boldsymbol{y}) = \frac{1}{2}(H_{kmn,y_l} + H_{lmn,y_k}) = H_{(k,y_l)mn},$$

$$B_{kljmn}(\boldsymbol{y}) = \frac{1}{2}(P_{kjmn,y_l} + P_{ljmn,y_k}) = P_{(k,y_l)jmn}, \tag{11}$$

$$\theta(\boldsymbol{y}) = \rho(\boldsymbol{y})/\rho_0, \quad \rho_0 = \langle \rho \rangle, \quad D_{ijmn}^0 = \langle C_{ijmn}^0(\boldsymbol{y}) \rangle, \tag{12}$$

and

$$\langle \cdot \rangle = |Y|^{-1} \int_Y \cdot \, dY , \tag{13}$$

is the averaging operator. $\boldsymbol{H}$ and $\boldsymbol{P}$ are normalized as

$$\langle H_{kmn}(\boldsymbol{y}) \rangle = 0 , \quad \langle P_{ijmn}(\boldsymbol{y}) \rangle = 0 . \tag{14}$$

Finite element method is utilized for the discretization of $\boldsymbol{H}$ and $\boldsymbol{P}$, which yields a set of linear algebraic systems with 6 right-hand-side vectors for $\boldsymbol{H}$ and 18 right-hand-side vectors for $\boldsymbol{P}$ (3 and 6 right-hand-side vectors, respectively, for the 2D case) [8].

For simplicity, attention is restricted to the constant mass density, in which case the macroscopic equations of motion up to $O(\varepsilon^2)$ are given as ([2]-[6])

$$\rho_0 u^0_{i,t_0t_0} - D^0_{ijmn}(e_{xmn}(\boldsymbol{u}^0))_{,x_j} = 0 , \tag{15}$$

$$\rho_0 U^1_{i,t_0t_0} - D^0_{ijmn}(e_{xmn}(\boldsymbol{U}^1))_{,x_j} = D^1_{ijkmn}(e_{xmn}(\boldsymbol{u}^0))_{,x_kx_j} - 2\rho_0 u^0_{i,t_0t_1} , \tag{16}$$

$$\rho_0 U^2_{i,t_0t_0} - D^0_{ijmn}(e_{xmn}(\boldsymbol{U}^2))_{,x_j} = D^2_{ijprmn}(e_{xmn}(\boldsymbol{u}^0))_{,x_rx_px_j} +$$

$$D^1_{ijrmn}(e_{xmn}(\boldsymbol{U}^1))_{,x_rx_j} - 2\rho_0 U^1_{i,t_0t_1} - 2\rho_0 u^0_{i,t_0t_2} - \rho_0 u^0_{i,t_1t_1} , \tag{17}$$

with initial and boundary conditions

$$\text{ICs:} \quad u^0_i(\boldsymbol{x}, 0, 0, 0) = p_i(\boldsymbol{x}) , \quad \dot{u}^0_i(\boldsymbol{x}, 0, 0, 0) = g_i(\boldsymbol{x}) , \tag{18}$$

$$U^s_i(\boldsymbol{x}, 0, 0, 0) = 0 , \quad \dot{U}^s_i(\boldsymbol{x}, 0, 0, 0) = 0 , \quad (s = 1, 2) , \tag{19}$$

$$\text{BCs:} \quad u^0_i = \bar{u}_i \quad \text{on } \Gamma_u ; \quad [D^0_{ijkl} e_{xkl}(\boldsymbol{u}^0)] n_j = \bar{h}_i \quad \text{on } \Gamma_\sigma , \tag{20}$$

$$U^s_i = 0 , \ \text{on } \Gamma_u ; \quad [D^0_{ijkl} e_{xkl}(\boldsymbol{U}^s)] n_j = 0 \quad \text{on } \Gamma_\sigma \qquad (s = 1, 2) , \tag{21}$$

where

$$D^1_{ijklm} = \langle C^1_{ijklm}(\boldsymbol{y}) \rangle = \langle C^0_{krij} H_{rlm} - C^0_{krlm} H_{rij} \rangle , \tag{22}$$

$$D^2_{ijklmn} = R_{ijklmn} + S_{ijklmn} , \tag{23}$$

$$R_{ijklmn} = \langle B_{stlmn} C_{stab} B_{abkij} \rangle - \langle H_{sij} C_{sklr} H_{rmn} \rangle , \quad S_{ijklmn} = \langle H_{aij} H_{als} \rangle D^0_{skmn} . \tag{24}$$

For symmetry properties of the macroscopic constitutive tensors, we refer to references [9], [11] and [6].

2.2 Nonlocal dispersive models

By introducing the averaged displacement

$$U_i(\boldsymbol{x}, t) = \langle u_i(\boldsymbol{x}, \boldsymbol{y}, t)\rangle = u_i^0 + \varepsilon U_i^1 + \varepsilon^2 U_i^2 + \dots , \tag{25}$$

and multiplying equations (16) and (17) by ε and ε^2, respectively, then adding the resulting equations to the leading-order equation (15) yields

$$\rho_0 \ddot{U}_i - D^0_{ijmn}(e_{xmn}(\boldsymbol{U}))_{,x_j} - \varepsilon D^1_{ijkmn}(e_{xmn}(\boldsymbol{U}))_{,x_k x_j} - \varepsilon^2 D^2_{ijprmn}(e_{xmn}(\boldsymbol{U}))_{,x_r x_p x_j} = 0 , \tag{26}$$

where terms of $O(\varepsilon^3)$ and higher are neglected and the relation between the full time derivative and partial derivatives with respect to different time scales is exploited. Equation (26) gives rise to the imaginary wave speed for higher wave numbers. This phenomenon is subsequently referred to as solution instability.

In absence of the polarization effect [11] ($\boldsymbol{D}^1 = 0$) and neglecting $\boldsymbol{R}$ in $\boldsymbol{D}^2$, equation (26) can be transformed into the so-called "good" Boussinesq equation [5]

$$\rho_0 \ddot{U}_i - D^0_{ijkl}(e_{xkl}(\boldsymbol{U}))_{,x_j} - \rho_0 E^0_{ijkl} \ddot{U}_{l,x_k x_j} = 0 , \tag{27}$$

where

$$E^0_{ijkl} = \varepsilon^2 \langle H_{mij} H_{mkl}\rangle . \tag{28}$$

Equation (27) is stable for any wave number and requires only C^0 continuity. However, since the sixth order tensor $\boldsymbol{R}$ has been neglected, the formulation is only valid for microstructures with negligible value of $\boldsymbol{R}$. For problems where the magnitude of $\boldsymbol{R}$ is comparable to that of $\boldsymbol{S}$ in $\boldsymbol{D}^2$, the model has been found to be inaccurate [6][10].

Beginning with equation (26) and neglecting the polarization effect ($\boldsymbol{D}^1 = 0$), Nagai *et al.* [6][10] developed a stabilized nonlocal model based on the three-field mixed variational formulation with assumed nonlocal stresses and strains. The model has been validated for plane harmonic analysis and for transient wave propagation in semi-infinite domain with different microstructures. Nevertheless, the issues of missing boundary conditions and wave reflection has not been fully addressed.

3.0 Reformulation of Macroscopic Equations

The nonlocal model (26) has been constructed to eliminate the slow time scales from the macroscopic equations of motion. And yet, in the process of substituting three higher order macroscopic equilibrium equations by a single nonlocal ideation an indispensable information has been lost giving rise to aforementioned shortcoming of the nonlocal model.

In the present manuscript, an alternative approach is pursued. We begin from the homogenized macroscopic equations of motion (15)-(17) without combining them into a single (nonlocal) equation of motion. From the weak form of the macroscopic equations the terms causing solution secularity are enforced to vanish giving rise to the governing equations of motion subjected to the secularity constrains. The weak form for the leading term, $\boldsymbol{u}^0$, is subsequently formulated. Finite element semidiscretization in space along with an analytical solution in slow time scales and Pade approximation in fast time scale are employed.

3.1 The Weak Form of macroscopic equations

The Weak Form of the macroscopic equations of motion (15)-(17) is given as follows:

For $t \in (0, T]$, find $u_i^0(\boldsymbol{x}, t_0, t_1, t_2) \in H^2(\Omega)$ and $U_i^s(\boldsymbol{x}, t_0, t_1, t_2) \in H^2(\Omega)$, $(s = 1, 2)$ which satisfy boundary conditions (20) and (21), such that $\forall w_i(\boldsymbol{x}) \in H_0^2(\Omega)$

$$\int_\Omega \rho_0 w_i u^0_{i,t_0t_0} d\Omega - \int_\Omega w_i D^0_{ijmn}(e_{xmn}(\boldsymbol{u}^0))_{,x_j} d\Omega = 0, \tag{29}$$

$$\int_\Omega \rho_0 w_i U^1_{i,t_0t_0} d\Omega - \int_\Omega w_i D^0_{ijmn}(e_{xmn}(\boldsymbol{U}^1))_{,x_j} d\Omega$$

$$= \int_\Omega w_i D^1_{ijkmn}(e_{xmn}(\boldsymbol{u}^0))_{,x_kx_j} d\Omega - 2\rho_0 \int_\Omega w_i u^0_{i,t_0t_1} d\Omega, \tag{30}$$

$$\int_\Omega \rho_0 w_i U^2_{i,t_0t_0} d\Omega - \int_\Omega w_i D^0_{ijmn}(e_{xmn}(\boldsymbol{U}^2))_{,x_j} d\Omega = \int_\Omega w_i D^2_{ijprmn}(e_{xmn}(\boldsymbol{u}^0))_{,x_rx_px_j} d\Omega +$$

$$\int_\Omega w_i D^1_{ijrmn}(e_{xmn}(\boldsymbol{U}^1))_{,x_rx_j} d\Omega - \rho_0 \int_\Omega w_i (2U^1_{i,t_0t_1} + 2u^0_{i,t_0t_2} + u^0_{i,t_1t_1}) d\Omega, \tag{31}$$

with

$$u_i^0(\boldsymbol{x}, 0, 0, 0) = p_i(\boldsymbol{x}), \quad \dot{u}_i^0(\boldsymbol{x}, 0, 0, 0) = g_i(\boldsymbol{x}),$$

$$U_i^s(\boldsymbol{x}, 0, 0, 0) = 0, \quad \dot{U}_i^s(\boldsymbol{x}, 0, 0, 0) = 0, \quad (s = 1, 2), \tag{32}$$

where $H^2(\Omega)$ is the Sobolev space defined as

$$H^2(\Omega) = \left\{ \boldsymbol{v} = \boldsymbol{v}(\boldsymbol{x}), \boldsymbol{x} \in \Omega | \boldsymbol{v}, \boldsymbol{v}_{,x_i}, \boldsymbol{v}_{,x_i x_j} \in L^2(\Omega) \right\}, \tag{33}$$

with $L^2(\Omega)$ denoting the set of square-integrable functions over Ω, and

$$H_0^2(\Omega) = \{ \boldsymbol{w}(\boldsymbol{x}) \in H^2(\Omega) \big| \boldsymbol{w}(\boldsymbol{x}) = 0 \text{ on } \Gamma_u, \partial \boldsymbol{w} / \partial \boldsymbol{n} = 0 \text{ on } \Gamma_\sigma \}, \tag{34}$$

where $\boldsymbol{n}$ is the direction of the unit outward normal to Γ. Integrating equations (29), (30) and (31) by parts yields

$$\int_\Omega \rho_0 w_i u^0_{i,t_0 t_0} d\Omega + \int_\Omega e_{xij}(\boldsymbol{w}) D^0_{ijmn} e_{xmn}(\boldsymbol{u}^0) d\Omega = \int_{\Gamma_\sigma} w_i \bar{h}_i dS, \tag{35}$$

$$\int_\Omega \rho_0 w_i U^1_{i,t_0 t_0} d\Omega + \int_\Omega e_{xij}(\boldsymbol{w}) D^0_{ijmn} e_{xmn}(\boldsymbol{U}^1) d\Omega = \int_\Gamma w_i D^1_{ijkmn} (e_{xmn}(\boldsymbol{u}^0))_{,x_k} n_j dS -$$

$$\int_\Omega e_{xij}(\boldsymbol{w}) D^1_{ijkmn} (e_{xmn}(\boldsymbol{u}^0))_{,x_k} d\Omega - 2\rho_0 \int_\Omega w_i u^0_{i,t_0 t_1} d\Omega, \tag{36}$$

$$\int_\Omega \rho_0 w_i U^2_{i,t_0 t_0} d\Omega + \int_\Omega e_{xij}(\boldsymbol{w}) D^0_{ijmn} e_{xmn}(\boldsymbol{U}^2) d\Omega = \int_\Gamma w_i D^2_{ijprmn} (e_{xmn}(\boldsymbol{u}^0))_{,x_r x_p} n_j dS$$

$$- \int_\Gamma e_{xij}(\boldsymbol{w}) D^2_{ijprmn} (e_{xmn}(\boldsymbol{u}^0))_{,x_r} n_p dS + \int_\Gamma w_i D^1_{ijrmn} (e_{xmn}(\boldsymbol{U}^1))_{,x_r} n_j dS$$

$$+ \int_\Omega (e_{xij}(\boldsymbol{w}))_{,x_p} D^2_{ijprmn} (e_{xmn}(\boldsymbol{u}^0))_{,x_r} d\Omega - \int_\Omega e_{xij}(\boldsymbol{w}) D^1_{ijrmn} (e_{xmn}(\boldsymbol{U}^1))_{,x_r} d\Omega$$

$$- \rho_0 \int_\Omega w_i (2U^1_{i,t_0 t_1} + 2u^0_{i,t_0 t_2} + u^0_{i,t_1 t_1}) d\Omega, \tag{37}$$

where

$$e_x(\boldsymbol{w}) = \nabla_x^s \boldsymbol{w} = \frac{1}{2} [\nabla_x \boldsymbol{w} + (\nabla_x \boldsymbol{w})^T], \tag{38}$$

is the symmetric gradient of $\boldsymbol{w}$.

3.2 Elimination of secularity

The right-hand-side of equation (36) contains solution to the associated homogeneous equations of motion, which give rise to secularity. In order to eliminate the secularity we enforce

$$\int_{\Gamma} w_i D^1_{ijkmn}(e_{xmn}(\boldsymbol{u}^0))_{,x_k} n_j dS = 0, \tag{39}$$

$$\int_{\Omega} [e_{xij}(\boldsymbol{w}) D^1_{ijkmn}(e_{xmn}(\boldsymbol{u}^0))_{,x_k} + 2\rho_0 w_i u^0_{i,t_0t_1}] d\Omega = 0. \tag{40}$$

With the vanishing forcing terms and quiescent initial conditions, it follows that $\boldsymbol{U}^1 \equiv 0$.

Likewise, the terms giving rise to the secularity in equation (37) are enforced to vanish

$$\int_{\Gamma} w_i D^2_{ijprmn}(e_{xmn}(\boldsymbol{u}^0))_{,x_r x_p} n_j dS = 0, \quad \int_{\Gamma} e_{xij}(\boldsymbol{w}) D^2_{ijprmn}(e_{xmn}(\boldsymbol{u}^0))_{,x_r} n_p dS = 0, \tag{41}$$

$$\int_{\Omega} (e_{xij}(\boldsymbol{w}))_{,x_p} D^2_{ijprmn}(e_{xmn}(\boldsymbol{u}^0))_{,x_r} d\Omega - \rho_0 \int_{\Omega} w_i (2u^0_{i,t_0t_2} + u^0_{i,t_1t_1}) d\Omega = 0. \tag{42}$$

and in combination with quiescent initial conditions we get $\boldsymbol{U}^2 \equiv 0$.

Equations (39) and (41) must be satisfied for any admissible function $\boldsymbol{w}$, so that we have the following natural boundary conditions

$$\bar{b}_i = D^1_{ijkmn}(e_{xmn}(\boldsymbol{u}^0))_{,x_k} n_j = 0, \quad \bar{c}_i = D^2_{ijprmn}(e_{xmn}(\boldsymbol{u}^0))_{,x_r x_p} n_j = 0 \text{ on } \Gamma_\sigma; \tag{43}$$

$$\bar{T}_{ij} = D^2_{ijprmn}(e_{xmn}(\boldsymbol{u}^0))_{,x_r} n_p = 0 \text{ on } \Gamma. \tag{44}$$

From equations (35), (40) and (42)-(44), the Strong Form for the leading term, $\boldsymbol{u}^0$, can now be reformulated as follows:

$$\rho_0 u^0_{i,t_0t_0} - D^0_{ijmn}(e_{xmn}(\boldsymbol{u}^0))_{,x_j} = 0, \tag{45}$$

with secularity constrains:

$$D^1_{ijkmn}(e_{xmn}(\boldsymbol{u}^0))_{,x_k x_j} - 2\rho_0 u^0_{i,t_0t_1} = 0, \tag{46}$$

$$D^2_{ijprmn}(e_{xmn}(\boldsymbol{u}^0))_{,x_r x_p x_j} - \rho_0 (2u^0_{i,t_0t_2} + u^0_{i,t_1t_1}) = 0, \tag{47}$$

and initial-boundary conditions:

$$u^0_i(\boldsymbol{x}, 0, 0, 0) = p_i(\boldsymbol{x}), \quad \dot{u}^0_i(\boldsymbol{x}, 0, 0, 0) = g_i(\boldsymbol{x}), \tag{48}$$

$$u_i^0 = \bar{u}_i \quad \text{on } \Gamma_u, \quad [D_{ijkl}^0 e_{xkl}(\boldsymbol{u}^0)]n_j = \bar{h}_i \quad \text{on } \Gamma_\sigma \tag{49}$$

$$\bar{b}_i = 0, \quad \bar{c}_i = 0 \text{ on } \Gamma_\sigma; \quad \bar{T}_{ij} = 0 \text{ on } \Gamma. \tag{50}$$

Remark 1: The secularity constrains (46)(47) and the boundary conditions (50) are closely related to the higher order stress equilibrium and surface traction equations [7].

3.3 Finite element semidiscretization in space

The Weak Form of equation (45) with secularity constrains (46) and (47) is given as follows:

For $t \in (0, T]$, find $u_i^0(\boldsymbol{x}, t_0, t_1, t_2) \in H^2(\Omega)$, which satisfies $u_i^0 = \bar{u}_i$ on Γ_u and $[D_{ijkl}^0 e_{xkl}(\boldsymbol{u}^0)]n_j = \bar{h}_i$ on Γ_σ, such that $\forall w_i(\boldsymbol{x}) \in H_0^2(\Omega)$

$$\int_\Omega \rho_0 w_i u_{i,t_0t_0}^0 d\Omega - \int_\Omega w_i D_{ijmn}^0 (e_{xmn}(\boldsymbol{u}^0))_{,x_j} d\Omega = 0, \tag{51}$$

subjected to the Weak Form of the secularity constrains

$$\int_\Omega w_i D_{ijkmn}^1 (e_{xmn}(\boldsymbol{u}^0))_{,x_k x_j} d\Omega - 2\rho_0 \int_\Omega w_i u_{i,t_0t_1}^0 d\Omega = 0, \tag{52}$$

$$\int_\Omega w_i D_{ijprmn}^2 (e_{xmn}(\boldsymbol{u}^0))_{,x_r x_p x_j} d\Omega - \rho_0 \int_\Omega w_i (2u_{i,t_0t_2}^0 + u_{i,t_1t_1}^0) d\Omega = 0. \tag{53}$$

Integrating equations (51)-(53) by parts and utilizing boundary conditions (50) yields

$$\int_\Omega \rho_0 w_i u_{i,t_0t_0}^0 d\Omega + \int_\Omega e_{xij}(\boldsymbol{w}) D_{ijmn}^0 e_{xmn}(\boldsymbol{u}^0) d\Omega = \int_{\Gamma_\sigma} w_i \bar{h}_i dS, \tag{54}$$

$$\int_\Omega e_{xij}(\boldsymbol{w}) D_{ijkmn}^1 (e_{xmn}(\boldsymbol{u}^0))_{,x_k} d\Omega + 2\rho_0 \int_\Omega w_i u_{i,t_0t_1}^0 d\Omega = 0, \tag{55}$$

$$\int_\Omega (e_{xij}(\boldsymbol{w}))_{,x_p} D_{ijprmn}^2 (e_{xmn}(\boldsymbol{u}^0))_{,x_r} d\Omega - \rho_0 \int_\Omega w_i (2u_{i,t_0t_2}^0 + u_{i,t_1t_1}^0) d\Omega = 0. \tag{56}$$

Employing the C^1 continuous finite element semi-discretization yields the semi-discrete equations of motion

$$\boldsymbol{M}\boldsymbol{d}_{,t_0t_0} + \boldsymbol{K}\boldsymbol{d} = \boldsymbol{F}(t), \tag{57}$$

subjected to the semi-discrete secularity constrains

$$\boldsymbol{K}_p\boldsymbol{d} + 2\varepsilon\boldsymbol{M}\boldsymbol{d}_{,t_0t_1} = \boldsymbol{0}\,, \quad \boldsymbol{K}_d\boldsymbol{d} - \varepsilon^2(2\boldsymbol{M}\boldsymbol{d}_{,t_0t_2} + \boldsymbol{M}\boldsymbol{d}_{,t_1t_1}) = \boldsymbol{0}\,, \tag{58}$$

and initial conditions

$$\boldsymbol{d}(0,0,0) = \boldsymbol{d}_0\,, \quad \dot{\boldsymbol{d}}(0,0,0) = \boldsymbol{v}_0\,, \tag{59}$$

where $\boldsymbol{d}$ is the global displacement vector; $\boldsymbol{M}$ and $\boldsymbol{K}$ are the global mass and stiffness matrices, respectively; $\boldsymbol{F}(t)$ is the external force vector; $\boldsymbol{K}_p$ and $\boldsymbol{K}_d$ are the global polarization and dispersion stiffness matrices, respectively, given as:

$$\boldsymbol{M} = \{M_{AE}\} = \mathop{\mathcal{A}}_{e=1}^{Ne} \int_{\Omega_e} \rho_0 N_{iA}^T N_{iE} d\Omega_e\,, \quad \boldsymbol{K} = \{K_{AE}\} = \mathop{\mathcal{A}}_{e=1}^{Ne} \int_{\Omega_e} B_{ijA}^T D_{ijmn}^0 B_{mnE} d\Omega_e\,,$$

$$\boldsymbol{F}(t) = \mathop{\mathcal{A}}_{e=1}^{Se} \int_{\Gamma_\sigma^e} \boldsymbol{N}^T \bar{\boldsymbol{h}} dS_e\,, \quad \boldsymbol{K}_p = \{K_{AE}\}_p = \mathop{\mathcal{A}}_{e=1}^{Ne} \int_{\Omega_e} B_{ijA}^T (\varepsilon D_{ijkmn}^1) \tilde{B}_{mnkE} d\Omega_e\,,$$

$$\boldsymbol{K}_d = \{K_{AE}\}_d = \mathop{\mathcal{A}}_{e=1}^{Ne} \int_{\Omega_e} \tilde{B}_{Akij}^T (\varepsilon^2 D_{ijklmn}^{2s}) \tilde{B}_{Emnl} d\Omega_e\,. \tag{60}$$

The capital subscripts denote degrees-of-freedom; the lower case subscripts stand for spatial dimensions ranging from 1 to 3 in 3D (or 1 to 2 in 2D). $\boldsymbol{N}$, $\boldsymbol{B}$ and $\tilde{\boldsymbol{B}}$ are element shape functions, strain-displacement, and strain gradient-displacement matrices, respectively, defined as

$$u_i^0(\boldsymbol{x}) = N_{iA} d_A^e\,, \quad B_{klA} = \frac{1}{2}(N_{kA,l} + N_{lA,k})\,, \quad \tilde{B}_{klmA} = \frac{1}{2}(N_{kA,lm} + N_{lA,km})\,. \tag{61}$$

Remark 2: The homogenized tensors $\varepsilon\boldsymbol{D}^1$ and $\varepsilon^2\boldsymbol{D}^{2s}$ can be directly calculated from the known geometry and micromechanical material properties in the unit cell, independently of the value of ε.

4.0 Time Integration

The semi-discrete governing equations (57)-(59) can be integrated numerically, but would require three-dimensional solution in t_0,t_1, t_2, which would significantly entail the overall computational cost. Instead, we construct an analytical solution for slow time scales

(t_1, t_2) and utilize Pade approximation to develop time stepping schemes on the fast time scale.

4.1 Analytical solution for the slow time scales

Define

$$\boldsymbol{z} = \begin{Bmatrix} \boldsymbol{d} \\ \boldsymbol{d}_{,t_0} \end{Bmatrix} \tag{62}$$

then equations (57) and (58) can be expressed as a first-order differential equation

$$\boldsymbol{z}_{,t_0} = \boldsymbol{A}\boldsymbol{z} + \boldsymbol{f}(t) \ , \tag{63}$$

with secularity constrains

$$\boldsymbol{B}_p \boldsymbol{z} + \varepsilon \boldsymbol{G} \boldsymbol{z}_{,t_1} = \boldsymbol{0} \ , \qquad \boldsymbol{B}_d \boldsymbol{z}_{,t_0} - \varepsilon^2 \boldsymbol{G}(2\boldsymbol{z}_{,t_0 t_2} + \boldsymbol{z}_{,t_1 t_1}) = \boldsymbol{0} \ , \tag{64}$$

and initial conditions

$$\boldsymbol{z}(0, 0, 0) = \begin{Bmatrix} \boldsymbol{d}_0 \\ \boldsymbol{v}_0 \end{Bmatrix} = \boldsymbol{C}_0 , \tag{65}$$

where

$$\boldsymbol{A} = \begin{bmatrix} \boldsymbol{0} & \boldsymbol{I} \\ -\boldsymbol{M}^{-1}\boldsymbol{K} & \boldsymbol{0} \end{bmatrix}, \qquad \boldsymbol{B}_p = \begin{bmatrix} \boldsymbol{0} & \boldsymbol{0} \\ \frac{1}{2}\boldsymbol{K}_p & \boldsymbol{0} \end{bmatrix}, \qquad \boldsymbol{B}_d = \begin{bmatrix} \boldsymbol{0} & \boldsymbol{0} \\ \boldsymbol{K}_d & \boldsymbol{0} \end{bmatrix},$$

$$\boldsymbol{G} = \begin{bmatrix} \boldsymbol{0} & \boldsymbol{0} \\ \boldsymbol{0} & \boldsymbol{M} \end{bmatrix}, \qquad \boldsymbol{f}(t) = \begin{Bmatrix} \boldsymbol{0} \\ \boldsymbol{M}^{-1}\boldsymbol{F}(t) \end{Bmatrix} . \tag{66}$$

Taking the Laplace transform of equation (63) with respect to t_0 yields

$$s\bar{\boldsymbol{z}}(s, t_1, t_2) - \boldsymbol{C}(t_1, t_2) = \boldsymbol{A}\bar{\boldsymbol{z}}(s, t_1, t_2) + \bar{\boldsymbol{f}}(s) \ , \tag{67}$$

where s is the transform (complex) variable and

$$\boldsymbol{C}(0, 0) = \boldsymbol{C}_0 . \tag{68}$$

From equation (67) we have

$$\bar{\boldsymbol{z}}(s, t_1, t_2) \;=\; (s\boldsymbol{I} - \boldsymbol{A})^{-1}\boldsymbol{C}(t_1, t_2) + (s\boldsymbol{I} - \boldsymbol{A})^{-1}\bar{\boldsymbol{f}}(s) \;. \tag{69}$$

Taking the inverse Laplace transform of the above equation yields

$$\boldsymbol{z}(t_0, t_1, t_2) \;=\; e^{\boldsymbol{A}t_0}\boldsymbol{C}(t_1, t_2) + \int_0^{t_0} e^{\boldsymbol{A}(t_0-\lambda)}\boldsymbol{f}(\lambda)d\lambda \;, \tag{70}$$

where the convolution theorem has been used for the last term.

Remark 3: The integral term in equation (70) is due to the particular solution to the leading order equations of motion (63). The particular solution does not generate secularity in the first and second order equations of motion and therefore it is convenient to remove it from the consideration of secularity constrains.

Substituting the first term in equation (70) into the secularity constrains (64) and making use of (63) yields

$$\boldsymbol{B}_p e^{\boldsymbol{A}t_0}\boldsymbol{C}(t_1, t_2) + \varepsilon\boldsymbol{G}e^{\boldsymbol{A}t_0}\boldsymbol{C}_{,t_1} \;=\; \boldsymbol{0} \;, \tag{71}$$

$$\boldsymbol{B}_d\boldsymbol{A}e^{\boldsymbol{A}t_0}\boldsymbol{C}(t_1, t_2) - 2\varepsilon^2\boldsymbol{G}\boldsymbol{A}e^{\boldsymbol{A}t_0}\boldsymbol{C}_{,t_2} - \varepsilon^2\boldsymbol{G}e^{\boldsymbol{A}t_0}\boldsymbol{C}_{,t_1t_1} + \boldsymbol{B}_d\boldsymbol{f}(t) \;=\; \boldsymbol{0} \;. \tag{72}$$

From equation (66) it is a trivial exercise to show that the following relations hold:

$$\boldsymbol{B}_d\boldsymbol{f}(t) \;=\; \boldsymbol{0} \;, \qquad \boldsymbol{B}_p\boldsymbol{f}(t) \;=\; \boldsymbol{0} \;. \tag{73}$$

The solution to equations (71) and (72) can be sought in the following form

$$e^{\boldsymbol{A}t_0}\boldsymbol{C}(t_1, t_2) \;=\; e^{\boldsymbol{A}t_0 + \boldsymbol{H}_1t_1/\varepsilon + \boldsymbol{H}_2t_2/\varepsilon^2}\boldsymbol{C}_0 \;, \tag{74}$$

where $\boldsymbol{H}_1$ and $\boldsymbol{H}_2$ are two matrices yet to be determined. The initial conditions are satisfied automatically.

Substituting equations (74) and (73) into (71) and (72), and accounting for the relations $e^{\boldsymbol{A}t_0}\boldsymbol{C}_{,t_1} \;=\; (e^{\boldsymbol{A}t_0}\boldsymbol{C})_{,t_1}$, $e^{\boldsymbol{A}t_0}\boldsymbol{C}_{,t_2} \;=\; (e^{\boldsymbol{A}t_0}\boldsymbol{C})_{,t_2}$ and $e^{\boldsymbol{A}t_0}\boldsymbol{C}_{,t_1t_1} \;=\; (e^{\boldsymbol{A}t_0}\boldsymbol{C})_{,t_1t_1}$, yields

$$(\boldsymbol{B}_p + \boldsymbol{G}\boldsymbol{H}_1)e^{\boldsymbol{A}t_0 + \boldsymbol{H}_1t_1/\varepsilon + \boldsymbol{H}_2t_2/\varepsilon^2}\boldsymbol{C}_0 \;=\; \boldsymbol{0} \;,$$

$$(\boldsymbol{B}_d\boldsymbol{A} - 2\boldsymbol{G}\boldsymbol{A}\boldsymbol{H}_2 - \boldsymbol{G}\boldsymbol{H}_1^2)e^{\boldsymbol{A}t_0 + \boldsymbol{H}_1t_1/\varepsilon + \boldsymbol{H}_2t_2/\varepsilon^2}\boldsymbol{C}_0 \;=\; \boldsymbol{0} \;. \tag{75}$$

The above equations have to be satisfied for any vector of initial conditions $\boldsymbol{C}_0$ and non-singular matrix $e^{\boldsymbol{A}t_0 + \boldsymbol{H}_1 t_1/\varepsilon + \boldsymbol{H}_2 t_2/\varepsilon^2}$. Therefore, it follows from equation (75):

$$\boldsymbol{B}_p + \boldsymbol{G}\boldsymbol{H}_1 = \boldsymbol{0}, \qquad \boldsymbol{B}_d\boldsymbol{A} - 2\boldsymbol{G}\boldsymbol{A}\boldsymbol{H}_2 - \boldsymbol{G}\boldsymbol{H}_1^2 = \boldsymbol{0}. \tag{76}$$

From the above equations, we can solve for $\boldsymbol{H}_1$ and $\boldsymbol{H}_2$ as

$$\boldsymbol{H}_1 = \begin{bmatrix} \boldsymbol{0} & \boldsymbol{K}^{-1}\boldsymbol{K}_p/2 \\ -\boldsymbol{M}^{-1}\boldsymbol{K}_p/2 & \boldsymbol{0} \end{bmatrix}, \qquad \boldsymbol{H}_2 = \begin{bmatrix} \boldsymbol{0} & -\boldsymbol{K}^{-1}\boldsymbol{K}_{dp}/2 \\ \boldsymbol{M}^{-1}\boldsymbol{K}_{dp}/2 & \boldsymbol{0} \end{bmatrix}, \tag{77}$$

where

$$\boldsymbol{K}_{dp} = \boldsymbol{K}_d + \frac{1}{4}\boldsymbol{K}_p\boldsymbol{K}^{-1}\boldsymbol{K}_p . \tag{78}$$

Substituting equation (74) into (70) yields

$$z(t_0, t_1, t_2) = e^{\boldsymbol{A}t_0 + \boldsymbol{H}_1 t_1/\varepsilon + \boldsymbol{H}_2 t_2/\varepsilon^2}\boldsymbol{C}_0 + \int_0^{t_0} e^{\boldsymbol{A}(t_0-\lambda)}\boldsymbol{f}(\lambda)d\lambda . \tag{79}$$

Recalling that $t_0 = t$, $t_1 = \varepsilon t$ and $t_2 = \varepsilon^2 t$, we have from equation (79)

$$z(t) = e^{(\boldsymbol{A}+\boldsymbol{H})t}\boldsymbol{C}_0 + \int_0^{t} e^{\boldsymbol{A}(t-\lambda)}\boldsymbol{f}(\lambda)d\lambda , \tag{80}$$

where

$$\boldsymbol{H} = \boldsymbol{H}_1 + \boldsymbol{H}_2 . \tag{81}$$

Now that the secularity constrains have been satisfied and the solution dependence on the slow time scales has been accounted for in closed form, we proceed with the development of the integration scheme for the fast temporal scale (see equation (80)) using Pade approximation.

4.2 Time integration scheme

4.2.1 Time integration scheme for the unforced case

For clarity of the presentation we first consider the force-free case, $\boldsymbol{f}(t) = \boldsymbol{0}$, in which case equation (80) reduces to

$$\boldsymbol{z}(t) \;=\; e^{(\boldsymbol{A}+\boldsymbol{H})t}\boldsymbol{C}_0\,, \tag{82}$$

from which it follows

$$\boldsymbol{z}(t+\Delta t) \;=\; e^{(\boldsymbol{A}+\boldsymbol{H})\Delta t}e^{(\boldsymbol{A}+\boldsymbol{H})t}\boldsymbol{C}_0 \;=\; e^{(\boldsymbol{A}+\boldsymbol{H})\Delta t}\boldsymbol{z}(t)\;. \tag{83}$$

so that the value of the solution at the current time step is related to that of the previous step by

$$\boldsymbol{z}_{n+1} \;=\; e^{(\boldsymbol{A}+\boldsymbol{H})\Delta t}\boldsymbol{z}_n\,. \tag{84}$$

The exponential function $e^{\boldsymbol{A}t}$ can be approximated using the Pade approximation:

$$e^{\boldsymbol{A}t} \sim (\boldsymbol{I} + b_1\boldsymbol{A}t + b_2\boldsymbol{A}^2t^2 + \ldots + b_n\boldsymbol{A}^nt^n)^{-1}(\boldsymbol{I} + a_1\boldsymbol{A}t +$$

$$a_2\boldsymbol{A}^2t^2 + \ldots + a_m\boldsymbol{A}^mt^m) \;=\; \boldsymbol{P}_{mn}\,. \tag{85}$$

Most widely used are the following three variants:

$$\boldsymbol{P}_{11} \;=\; \left(\boldsymbol{I} - \frac{t}{2}\boldsymbol{A}\right)^{-1}\left(\boldsymbol{I} + \frac{t}{2}\boldsymbol{A}\right)\,,$$

$$\boldsymbol{P}_{12} \;=\; \left(\boldsymbol{I} - \frac{2}{3}\boldsymbol{A}t + \frac{1}{6}\boldsymbol{A}^2t^2\right)^{-1}\left(\boldsymbol{I} + \frac{1}{3}\boldsymbol{A}t\right)\,,$$

$$\boldsymbol{P}_{22} \;=\; \left(\boldsymbol{I} - \frac{1}{2}\boldsymbol{A}t + \frac{1}{12}\boldsymbol{A}^2t^2\right)^{-1}\left(\boldsymbol{I} + \frac{1}{2}\boldsymbol{A}t + \frac{1}{12}\boldsymbol{A}^2t^2\right)\,. \tag{86}$$

All three schemes are unconditionally stable [12][13]. Only the $\boldsymbol{P}_{11}$ scheme is sequential, in the sense that solution for displacement, velocity and acceleration vectors is uncoupled.

Using the $\boldsymbol{P}_{11}$ Pade approximation for $e^{(\boldsymbol{A}+\boldsymbol{H})\Delta t}$, we have from equation (84)

$$\left[\boldsymbol{I} - \frac{\Delta t}{2}(\boldsymbol{A}+\boldsymbol{H})\right]\boldsymbol{z}_{n+1} \;=\; \left[\boldsymbol{I} + \frac{\Delta t}{2}(\boldsymbol{A}+\boldsymbol{H})\right]\boldsymbol{z}_n\,. \tag{87}$$

Substituting expressions for $\boldsymbol{A}$ and $\boldsymbol{H}$ from equations (66), (77) and (81) into (87) yields

$$\boldsymbol{d}_{n+1} - \frac{\Delta t}{2}(\boldsymbol{I} - \boldsymbol{K}^{-1}\boldsymbol{K}_2)\boldsymbol{v}_{n+1} \;=\; \boldsymbol{d}_n + \frac{\Delta t}{2}(\boldsymbol{I} - \boldsymbol{K}^{-1}\boldsymbol{K}_2)\boldsymbol{v}_n\,,$$

$$\frac{\Delta t}{2}\boldsymbol{M}^{-1}(\boldsymbol{K}-\boldsymbol{K}_2)\boldsymbol{d}_{n+1}+\boldsymbol{v}_{n+1} = -\frac{\Delta t}{2}\boldsymbol{M}^{-1}(\boldsymbol{K}-\boldsymbol{K}_2)\boldsymbol{d}_n+\boldsymbol{v}_n \ , \tag{88}$$

where $\boldsymbol{v} = \boldsymbol{d}_{,t}$ is the velocity vector and

$$\boldsymbol{K}_2 = \frac{1}{2}(\boldsymbol{K}_{dp}-\boldsymbol{K}_p) \ . \tag{89}$$

From equation (88), we can solve for the displacement and velocity vectors independently:

$$\left(\boldsymbol{K}+\frac{\Delta t^2}{4}\tilde{\boldsymbol{K}}\boldsymbol{M}^{-1}\tilde{\boldsymbol{K}}\right)\boldsymbol{d}_{n+1} = \left(\boldsymbol{K}-\frac{\Delta t^2}{4}\tilde{\boldsymbol{K}}\boldsymbol{M}^{-1}\tilde{\boldsymbol{K}}\right)\boldsymbol{d}_n+\Delta t\tilde{\boldsymbol{K}}\boldsymbol{v}_n \ ,$$

$$\boldsymbol{v}_{n+1} = -\frac{\Delta t}{2}\boldsymbol{M}^{-1}\tilde{\boldsymbol{K}}(\boldsymbol{d}_n+\boldsymbol{d}_{n+1})+\boldsymbol{v}_n \ . \tag{90}$$

where

$$\tilde{\boldsymbol{K}} = \boldsymbol{K}-\boldsymbol{K}_2 \ . \tag{91}$$

Remark 4: For the special case of non-polarized and non-dispersive medium, $\boldsymbol{K}_p = \boldsymbol{0}$, $\boldsymbol{K}_d = \boldsymbol{0}$, and $\tilde{\boldsymbol{K}}$ reduces to $\boldsymbol{K}$. The first equation in (90) reduces to

$$\left(\boldsymbol{K}+\frac{4}{\Delta t^2}\boldsymbol{M}\right)\boldsymbol{d}_{n+1} = \frac{4}{\Delta t^2}\boldsymbol{M}\boldsymbol{d}_n-\boldsymbol{K}\boldsymbol{d}_n+\frac{4}{\Delta t}\boldsymbol{M}\boldsymbol{v}_n \ , \tag{92}$$

from which we have

$$\boldsymbol{M}^{-1}\boldsymbol{K}(\boldsymbol{d}_n+\boldsymbol{d}_{n+1}) = \frac{4}{\Delta t^2}(\boldsymbol{d}_n-\boldsymbol{d}_{n+1})+\frac{4}{\Delta t}\boldsymbol{v}_n \ . \tag{93}$$

Rewriting equation (92) using the force-free equations of motion at t_n, and substituting equation (93) into the reduced equation (90), we have

$$\left(\boldsymbol{K}+\frac{4}{\Delta t^2}\boldsymbol{M}\right)\boldsymbol{d}_{n+1} = \frac{4}{\Delta t^2}\boldsymbol{M}\boldsymbol{d}_n+\frac{4}{\Delta t}\boldsymbol{M}\boldsymbol{v}_n+\boldsymbol{M}\boldsymbol{a}_n \ ,$$

$$\boldsymbol{v}_{n+1} = \frac{2}{\Delta t}(\boldsymbol{d}_{n+1}-\boldsymbol{d}_n)-\boldsymbol{v}_n \ . \tag{94}$$

Equation (94) is the standard Newmark scheme with $\beta = 1/4$ and $\gamma = 1/2$ known as the trapezoidal rule [14].

4.2.2 Time integration scheme for the forced case

The forcing function $\boldsymbol{f}(t)$ is approximated as a set of piecewise linear segments [15]. In each interval $(t, t+\Delta t)$, we let $\boldsymbol{f}(t)$ be represented by

$$\boldsymbol{f}(\lambda) \sim \boldsymbol{f}_n + \frac{\lambda}{\Delta t}(\boldsymbol{f}_{n+1} - \boldsymbol{f}_n) \quad , \text{ in } \quad 0 \le \lambda \le \Delta t , \tag{95}$$

where $\boldsymbol{f}_n$ and $\boldsymbol{f}_{n+1}$ are the external force values at time t_n and $t_{n+1} = t_n + \Delta t$, respectively.

Based on the approximation of the forcing function (95), we can evaluate the following integration as:

$$\int_0^{\Delta t} e^{\boldsymbol{A}(\Delta t - \lambda)} \boldsymbol{f}(\lambda) d\lambda = e^{\boldsymbol{A}\Delta t}\boldsymbol{A}^{-1}\boldsymbol{f}_n - \boldsymbol{A}^{-1}\boldsymbol{f}_{n+1} + (e^{\boldsymbol{A}\Delta t} - \boldsymbol{I})\boldsymbol{A}^{-2}\frac{1}{\Delta t}(\boldsymbol{f}_{n+1} - \boldsymbol{f}_n) \quad . \tag{96}$$

Inserting the $\boldsymbol{P}_{11}$ Pade approximation for $e^{\boldsymbol{A}\Delta t}$ into equation (96) and pre-multiplying through by $(\boldsymbol{I} - \Delta t\boldsymbol{A}/2)$ yields

$$\left(\boldsymbol{I} - \frac{\Delta t}{2}\boldsymbol{A}\right)\int_0^{\Delta t} e^{\boldsymbol{A}(\Delta t - \lambda)} \boldsymbol{f}(\lambda) d\lambda = \frac{\Delta t}{2}(\boldsymbol{f}_n + \boldsymbol{f}_{n+1}) \quad . \tag{97}$$

From equation (80), we have

$$\boldsymbol{z}(\Delta t) = e^{(\boldsymbol{A}+\boldsymbol{H})\Delta t}\boldsymbol{C}_0 + \int_0^{\Delta t} e^{\boldsymbol{A}(\Delta t - \lambda)} \boldsymbol{f}(\lambda) d\lambda \ . \tag{98}$$

After $\boldsymbol{z}(\Delta t)$ is evaluated, it becomes the initial value for evaluating $\boldsymbol{z}(2\Delta t)$. Therefore, we have the relation between the values of two consecutive time steps:

$$\boldsymbol{z}_{n+1} = e^{(\boldsymbol{A}+\boldsymbol{H})\Delta t}\boldsymbol{z}_n + \int_0^{\Delta t} e^{\boldsymbol{A}(\Delta t - \lambda)} \boldsymbol{f}(\lambda) d\lambda \ . \tag{99}$$

Pre-multiplying equation (99) by $(\boldsymbol{I} - \Delta t\boldsymbol{A}/2)$ and making use of (97) yields

$$\left(\boldsymbol{I} - \frac{\Delta t}{2}\boldsymbol{A}\right)\boldsymbol{z}_{n+1} = \left(\boldsymbol{I} - \frac{\Delta t}{2}\boldsymbol{A}\right)e^{(\boldsymbol{A}+\boldsymbol{H})\Delta t}\boldsymbol{z}_n + \frac{\Delta t}{2}(\boldsymbol{f}_n + \boldsymbol{f}_{n+1}) \quad . \tag{100}$$

Using the $\boldsymbol{P}_{11}$ Pade approximation for $e^{(\boldsymbol{A}+\boldsymbol{H})\Delta t}$ in equation (100) and pre-multiplying the resulting equation by $[\boldsymbol{I} - (\boldsymbol{A}+\boldsymbol{H})\Delta t/2]$ yields

$$\left[\boldsymbol{I}-\frac{\Delta t}{2}(\boldsymbol{A}+\boldsymbol{H})\right]\left(\boldsymbol{I}-\frac{\Delta t}{2}\boldsymbol{A}\right)\boldsymbol{z}_{n+1} = \frac{\Delta t}{2}\left[\boldsymbol{I}-\frac{\Delta t}{2}(\boldsymbol{A}+\boldsymbol{H})\right](\boldsymbol{f}_n+\boldsymbol{f}_{n+1})+$$

$$\left[\boldsymbol{I}-\frac{\Delta t}{2}(\boldsymbol{A}+\boldsymbol{H})\right]\left(\boldsymbol{I}-\frac{\Delta t}{2}\boldsymbol{A}\right)\left[\boldsymbol{I}-\frac{\Delta t}{2}(\boldsymbol{A}+\boldsymbol{H})\right]^{-1}\left[\boldsymbol{I}+\frac{\Delta t}{2}(\boldsymbol{A}+\boldsymbol{H})\right]\boldsymbol{z}_n \ . \tag{101}$$

If equation (101) is used directly in the time integration, displacement and velocity vectors cannot be evaluated separately and they can only be solved in the coupled vector $\boldsymbol{z}$, with the degrees of freedom twice of the original finite element equations of motion. A more efficient implementation is as follows:

Equation (101) can be written as two equations

$$\left[\boldsymbol{I}-\frac{\Delta t}{2}(\boldsymbol{A}+\boldsymbol{H})\right]\boldsymbol{w}_{n+1} = \frac{\Delta t}{2}\left[\boldsymbol{I}-\frac{\Delta t}{2}(\boldsymbol{A}+\boldsymbol{H})\right](\boldsymbol{f}_n+\boldsymbol{f}_{n+1})+$$

$$\left[\boldsymbol{I}-\frac{\Delta t}{2}(\boldsymbol{A}+\boldsymbol{H})\right]\left(\boldsymbol{I}-\frac{\Delta t}{2}\boldsymbol{A}\right)\left[\boldsymbol{I}-\frac{\Delta t}{2}(\boldsymbol{A}+\boldsymbol{H})\right]^{-1}\left[\boldsymbol{I}+\frac{\Delta t}{2}(\boldsymbol{A}+\boldsymbol{H})\right]\boldsymbol{z}_n \ ,$$

$$\left(\boldsymbol{I}-\frac{\Delta t}{2}\boldsymbol{A}\right)\boldsymbol{z}_{n+1} = \boldsymbol{w}_{n+1} \ . \tag{102}$$

Let

$$\boldsymbol{w}_{n+1} = \begin{Bmatrix}\boldsymbol{q}_{n+1}\\ \boldsymbol{r}_{n+1}\end{Bmatrix}. \tag{103}$$

Using the expressions for matrices and vector $\boldsymbol{A}$, $\boldsymbol{H}$ and $\boldsymbol{f}(t)$ in equations (66), (77) and (81), we can evaluate

$$\boldsymbol{I}-\frac{\Delta t}{2}(\boldsymbol{A}+\boldsymbol{H}) = \begin{bmatrix}\boldsymbol{I} & -\Delta t\boldsymbol{K}^{-1}\tilde{\boldsymbol{K}}/2\\ \Delta t\boldsymbol{M}^{-1}\tilde{\boldsymbol{K}}/2 & \boldsymbol{I}\end{bmatrix},$$

$$\boldsymbol{I}+\frac{\Delta t}{2}(\boldsymbol{A}+\boldsymbol{H}) = \begin{bmatrix}\boldsymbol{I} & \Delta t\boldsymbol{K}^{-1}\tilde{\boldsymbol{K}}/2\\ -\Delta t\boldsymbol{M}^{-1}\tilde{\boldsymbol{K}}/2 & \boldsymbol{I}\end{bmatrix}, \quad \boldsymbol{I}-\frac{\Delta t}{2}\boldsymbol{A} = \begin{bmatrix}\boldsymbol{I} & -\Delta t\boldsymbol{I}/2\\ \Delta t\boldsymbol{M}^{-1}\boldsymbol{K}/2 & \boldsymbol{I}\end{bmatrix},$$

$$\left[\boldsymbol{I}-\frac{\Delta t}{2}(\boldsymbol{A}+\boldsymbol{H})\right]^{-1} = \begin{bmatrix} \boldsymbol{I}-\frac{\Delta t^2}{4}\boldsymbol{K}^{-1}\tilde{\boldsymbol{K}}\boldsymbol{M}^{-1}\tilde{\boldsymbol{K}}+O(\Delta t^4) & \frac{\Delta t}{2}\boldsymbol{K}^{-1}\tilde{\boldsymbol{K}}+O(\Delta t^3) \\ -\frac{\Delta t}{2}\boldsymbol{M}^{-1}\tilde{\boldsymbol{K}}+O(\Delta t^3) & \boldsymbol{I}-\frac{\Delta t^2}{4}\boldsymbol{M}^{-1}\tilde{\boldsymbol{K}}\boldsymbol{K}^{-1}\tilde{\boldsymbol{K}}+O(\Delta t^4) \end{bmatrix},$$

$$\frac{\Delta t}{2}\left[\boldsymbol{I}-\frac{\Delta t}{2}(\boldsymbol{A}+\boldsymbol{H})\right](\boldsymbol{f}_n+\boldsymbol{f}_{n+1}) = \begin{Bmatrix} -\Delta t^2\boldsymbol{K}^{-1}\tilde{\boldsymbol{K}}\boldsymbol{M}^{-1}(\boldsymbol{F}_n+\boldsymbol{F}_{n+1})/4 \\ \Delta t\boldsymbol{M}^{-1}(\boldsymbol{F}_n+\boldsymbol{F}_{n+1})/2 \end{Bmatrix}. \tag{104}$$

Since the $\boldsymbol{P}_{11}$ Pade approximation is second-order accurate, we can neglect terms of $O(\Delta t^3)$ and higher. Substituting equation (104) into (102) yields

$$\left(\boldsymbol{K}+\frac{\Delta t^2}{4}\tilde{\boldsymbol{K}}\boldsymbol{M}^{-1}\tilde{\boldsymbol{K}}\right)\boldsymbol{q}_{n+1} = \left(\boldsymbol{K}+\frac{\Delta t^2}{4}\tilde{\boldsymbol{K}}\boldsymbol{M}^{-1}\hat{\boldsymbol{K}}\right)\boldsymbol{d}_n+\frac{\Delta t}{2}\left[\boldsymbol{K}-2\boldsymbol{K}_2+\frac{\Delta t^2}{4}\tilde{\boldsymbol{K}}\boldsymbol{M}^{-1}\tilde{\boldsymbol{K}}\right]\boldsymbol{v}_n, \tag{105}$$

$$\boldsymbol{M}\boldsymbol{r}_{n+1} = -\frac{\Delta t}{2}(\tilde{\boldsymbol{K}}\boldsymbol{q}_{n+1}-\boldsymbol{K}_2\boldsymbol{d}_n)+\left(\boldsymbol{M}+\frac{\Delta t^2}{4}\tilde{\boldsymbol{K}}\right)\boldsymbol{v}_n+\frac{\Delta t}{2}(\boldsymbol{F}_n+\boldsymbol{F}_{n+1}), \tag{106}$$

$$\left(\boldsymbol{M}+\frac{\Delta t^2}{4}\boldsymbol{K}\right)\boldsymbol{d}_{n+1} = \boldsymbol{M}\boldsymbol{q}_{n+1}+\frac{\Delta t}{2}(\boldsymbol{M}\boldsymbol{r}_{n+1}), \tag{107}$$

$$\boldsymbol{v}_{n+1} = \boldsymbol{M}^{-1}\left[(\boldsymbol{M}\boldsymbol{r}_{n+1})-\frac{\Delta t}{2}\boldsymbol{K}\boldsymbol{d}_{n+1}\right], \tag{108}$$

where

$$\tilde{\boldsymbol{K}} = \boldsymbol{K}-\boldsymbol{K}_2, \quad \hat{\boldsymbol{K}} = \boldsymbol{K}+\boldsymbol{K}_2. \tag{109}$$

The time integration scheme becomes:

- Solve for $\boldsymbol{q}_{n+1}$ by equation (105) based on displacement and velocity values of the previous time step;
- Evaluate the vector $\boldsymbol{M}\boldsymbol{r}_{n+1}$ by equation (106);
- Solve for the displacement vector $\boldsymbol{d}_{n+1}$ of the current time step by equation (107);
- Evaluate the velocity vector $\boldsymbol{v}_{n+1}$ of the current time step by equation (108);
- Update the displacement and velocity vectors and the integration proceeds to the next time step.

The algorithm necessitates sequential solution of two systems of linear equations at each time step rather than solving a coupled system of linear equations with twice as many degrees-of-freedom.

5.0 Numerical Examples

We consider wave propagation in two-dimensional semi-infinite and finite domains. Two microstructures in plane strain setting have been analyzed.

5.1 Semi-infinite domain

The semi-infinite domain and the corresponding two microstructures are illustrated in Figure 1. The unit cells are composed of two material constituents with Young's modulus, Poisson's ratio and mass density as $E_1 = 60GPa$, $E_2 = 1GPa$, $\nu_1 = \nu_2 = 0.2$ and $\rho_1 = \rho_2 = 10^3 Kg/m^3$. In the vertical direction periodic boundary conditions are assumed. The left edge of the domain is fixed while the right edge is subjected to a distributed impact load in the horizontal or vertical directions in the form of the Sine-like pulse

$$P(t) = \begin{cases} P_0 a(t - T/2)[t(t-T)]^4 & 0 \le t \le T \\ 0 & t > T \end{cases} \tag{110}$$

where T denotes the pulse duration; P_0 is the amplitude of the pulse and a is scaled to $a = 3 \times 9^4/(8T^9)$, so that $-P_0 \le P(t) \le P_0$.

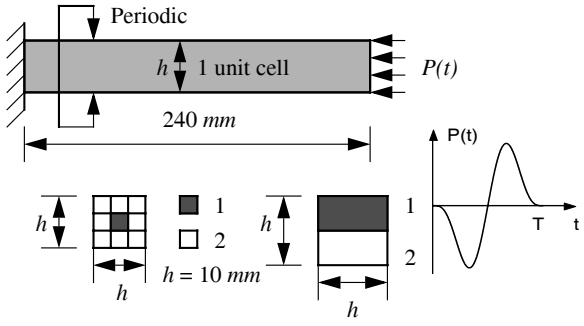

Figure 1: Semi-infinite domain and two microstructures

Both unit cells are discretized with 60×60 square-shaped bilinear finite elements to evaluate the homogenized constitutive tensors. For the checkerboard medium, the macro-domain is discretized using 3×72 four-node C^1 continuous elements. For the reference solution, the heterogeneous solid is discretized using 12×288 C^0 four-node square-shaped bilinear elements. To evaluate the response obtained by the classical homogenization, the macro-domain is discretized using 9×216 C^0 four-node square-shaped bilinear elements. The same discretization is used for the layered medium.

First, we consider a horizontally applied impact load with relatively long pulse duration $T = 2.1ms$. The time history of the horizontal displacement at the point $x = 120mm$,

$y = h/3$ obtained by the classic homogenization, the proposed multiscale approach and the reference solutions are plotted in Figure 2. It can be observed that for the relatively long pulse duration, i.e., low wave number for the traveling wave, the two approximation methods are in good agreement with the reference solution.

Figure 2: Horizontal displacements at $x = 120mm$, $y = h/3$ for the horizontal load (the checkerboard medium)

Next, we consider the cases of relatively short pulse durations. For the checkerboard medium we consider $T = 90\mu s$ and $T = 130\mu s$ for horizontally and vertically applied impact loading, respectively. For the layered medium we consider $T = 70\mu s$ and $T = 210\mu s$ for horizontally and vertically applied impact loading, respectively. For the checkerboard medium, the horizontal displacement for the horizontal loading and the vertical displacement for the vertical loading at the point $x = 120mm$, $y = h/3$ are plotted in Figure 3 and Figure 4, respectively. For the layered medium, the horizontal displacement for the horizontal loading and vertical displacement for the vertical loading at the point $x = 120mm$, $y = h/2$ are plotted in Figure 5 and Figure 6, respectively. It can be seen that the proposed multiscale model is in good agreement with the reference solution, whereas the classical homogenization exhibit considerable discrepancies.

5.2 Finite domain

The configuration of the finite domain and the microstructure is illustrated in Figure 7. The properties of the two material constituents are the same as in the case of semi-infinite domain. The left edge of the finite domain is fixed while the right edge is subjected to the distributed impact load in the horizontal direction in the form of the pulse given by equation (110). Figure 8 shows the horizontal displacements at the center of the domain for the pulse duration $T = 130\mu s$. It can be observed that the solution obtained by the proposed method is in good agreement with the response obtained by the reference solution, while the solution obtained by the classical homogenization exhibits significant deviations.

Figure 3. Horizontal displacements at $x = 120mm$, $y = h/3$ for the horizontal load (the checkerboard medium)

Figure 4. Vertical displacements at $x = 120mm$, $y = h/3$ for the vertical load (the checkerboard medium)

Figure 5: Horizontal displacements at $x = 120mm$, $y = h/2$ for the horizontal load (the layered medium)

Figure 6: Vertical displacements at $x = 120mm$, $y = h/2$ for the vertical load (the layered medium)

Figure 7: Finite domain and the microstructure

Figure 8: Horizontal displacements at the center for the horizontal load.

6.0 Conclusions and future work

A space-time multiscale model for wave propagation in heterogeneous media has been developed and verified on semi-infinite and finite domains. The model builds on the authors' previous work on the higher-order mathematical homogenization theory with multiple spatial and temporal scales ([4]-[6]), and is aimed at addressing the issues of stability and mathematical consistency. Starting from the weak forms of homogenized macroscopic equations of motion, terms causing the solution secularity are identified and enforced to vanish. This condition recovers the missing boundary conditions and gives rise to two secularity constrains imposing the uniform validity of asymptotic expansions. Finite element semidiscretization in space along with an analytical solution for slow time scales and Pade approximation for the fast time scale are employed.

Several issues have not been addressed and will be the main focus of our future investigation:

1. While the formulation is general, only weakly polarized media has been implemented and studied. If the polarization effects are significant, the polarization stiffness matrix $\boldsymbol{K}_p$ is asymmetric due to skew-symmetry of $\boldsymbol{D}^1$. Accounting for polarization effects would require consideration of nonsymmetric global stiffness matrices.

2. The governing macroscopic equations of motion (the Strong Form) involve the fourth-order spatial derivative requiring C^1 continuity of the solution in the Weak Form. In the present manuscript we implemented C^1 continuous elements in 2D. However, for the general 3D cases, C^1 elements are extremely difficult to develop, if not impossible. Various mixed formulations can be used instead, but the overhead compared to the C^0 single field variational formulation is substantial. In our future investigation we will consider application of the Continuous/Discontinuous Galerkin (C/DG) approximation developed by Engel *et al.* [21].

3. For numerical integration in fast time only implicit scheme has been investigated so far. For high strain rates applications an explicit scheme will be developed in our future work.

Acknowledgment

This work was supported by the Sandia National Laboratories under Contract DE-AL04-94AL8500 and the Office of Naval Research through grant number N00014-97-1-0687.

References

1 Botkin ME., Crash Prediction of Composite Structures. private communications, May, 2003.

2 Fish J. and Chen W., Higher-order homogenization of initial-boundary value problem. *J. Engng. Mech.*, 127(12): 1223-1230, 2001.

3 Chen W. and Fish J., A dispersive model for wave propagation in periodic heterogeneous media based on homogenization with multiple spatial and temporal scales. *J. Appl. Mech., Transaction of the ASME*, 68:153-161, 2001.

4 Fish J., Chen W. and Nagai G., Non-local dispersive model for wave propagation in heterogeneous media: one-dimensional case. *Int. J. Numer. Meth. Engng.*, 54:331-346, 2000.

5 Fish J., Chen W. and Nagai G., Non-local dispersive model for wave propagation in heterogeneous media: multi-dimensional case. *Int. J. Numer. Meth. Engng.*, 54:347-363, 2000.

6 Nagai G., Fish J. and Watanabe K., Stabilized nonlocal model for wave propagation in heterogeneous media. in print, *Comput. Mech.*, 2002.

7 Fleck NA. and Hutchinson JW., Strain Gradient Plasticity. *Advances in Applied Mechanics*, Vol. 33:295-361, 1997.

8 Fish J., Nayak P. and Holmes MH., Microscale reduction error indicators and estimators for a periodic heterogeneous medium. *Comput. Mech.,* 14:323-338, 1994.

9 Fish J. and Wagiman A., Multiscale finite element method for a locally nonperiodic heterogeneous medium. *Comput. Mech.*, 12:164-180, 1993.

10 Nagai G., Fish J. and Watanabe K., Stabilized non-local model for dispersive wave propagation in heterogeneous media. Proceedings of the Fifth World Congress on Computational Mechanics. Mang HA., Rammerstorfer FG. and Eberhardsteiner J. (Eds.), Vienna, Austria, July 7-12, 2002.

11 Boutin C., Microstructural effects in elastic composites. *Int. J. Solids Struct.,* 33(7):1023-1051, 1996.

12 Ruge P., Restricted Pade scheme in computational structural dynamics. *Computers & Structures*, 79:1913-1921, 2001.

13 Donea J., Roig B. and Huerta A., High-order accurate time-stepping schemes for convection-diffusion problems. *Comput. Methods Appl. Mech. Engrg.*, 182:249-275, 2000.

14 Hughes TJR., *The Finite Element Method, Linear Static and Dynamic Finite Element Analysis.* Prentice-Hall, Englewood Cliffs, New Jersey, 1987.

15 Trujillo DM., The direct numerical integration of linear matrix differential equations using Pade approximations. *Int. J. Numer. Meth. Engng.*, 9:259-270, 1975.

16 Ortega JM., *Matrix Theory, A Second Course.* Plenum Press, New York, 1989.

17 Lancaster P. and Tismenetsky M., *The Theory of Matrices.* 2nd Edition, Academic Press, Orlando, Florida, 1985.

18 Jain MC., *Vector Spaces and Matrices in Physics*. CRC Press, London, 2001.

19 Magid AR., *Applied Matrix Models*. John Wiley & Sons, New York,1985.

20 Hallquist JO., LS-DYNA Theoretical Manual, Livermore Software Technology Corporation, May 2001.

21 Engel G., Garikipati K., Hughes TJR., Larson MG., Mazzei L. and Taylor RL., Continuous/ discontinuous finite element approximations of fourth-order elliptic problems in structural and continuum mechanics with applications to thin beams and plates, and strain gradient elasticity, *Comput. Methods Appl. Mech. Engrg.*, 191:3669-3750, 2002.